

Fully Convolutional Network-based Multi-Task Learning for Rectum and Rectal Cancer Segmentation

Joohyung Lee¹, Ji Eun Oh¹, Min Ju Kim², Bo Yun Hur², Sun Ah Cho¹, and Dae Kyung Sohn^{1, 2*}

¹ *Innovative Medical Engineering & Technology, National Cancer Center,
Goyang-si, Gyeonggi-do 10408 South Korea*

² *Center for Colorectal Cancer, National Cancer Center,
Goyang-si, Gyeonggi-do 10408 South Korea*

Abstract

In this study, we present a fully automatic method to segment both rectum and rectal cancer based on Deep Neural Networks (DNNs) with axial T2-weighted Magnetic Resonance images. Clinically, the relative location between rectum and rectal cancer plays an important role in cancer treatment planning. Such a need motivates us to propose a fully convolutional architecture for Multi-Task Learning (MTL) to segment both rectum and rectal cancer. Moreover, we propose a bias-variance decomposition-based method which can visualize and assess regional robustness of the segmentation model. In addition, we also suggest a novel augmentation method which can improve the segmentation performance as well as reduce the training time.

Overall, our proposed method is not only computationally efficient due to its fully convolutional nature but also outperforms the current state-of-the-art for rectal cancer segmentation. It also scores high accuracy in rectum segmentation without any prior study reported. Moreover, we conclude that supplementing rectum information benefits the rectal cancer segmentation model, especially in model variance.

1. Introduction

Globally, colorectal cancer is the third most common cancer and the second leading cause of cancer mortality (Bhandari et al., 2017). Specifically, colorectal cancer was the most commonly diagnosed cancer in Korea for 2017 with 27,837 new cases (Jung et al., 2017). The global burden of colorectal cancer is rising fast and is expected to increase by 60% in 2030 (Arnold et al., 2017).

The Union for International Cancer Control TNM classification of Malignant Tumours (8th edition) categorizes rectal cancer as the tumor which starts in the rectum, the last 12 centimeters of the colon

(Gospodarowicz et al., 2017). Furthermore, the T-category of rectal cancer pathologically classifies the progression of rectal cancer by the degree of tumor invasion to the rectal wall. In the MR image, the T-category of rectal cancer can be determined by the relative location between the tumor and the rectal wall (Cho et al., 2017). Since the current treatment guidelines for rectal cancer recommend different treatments depending on the T-category of rectal cancer, accurate segmentation of rectum and rectal cancer is crucial. However, in practice, T-categorization by locating rectum and rectal cancer in MR image is done manually by radiologists. Manual localization is time-consuming, and a reliable auto-segmentation system is demanding (Trebeschi et al., 2017).

These days, Deep Learning has improved the state-of-the-art in various Computer Vision related fields (LeCun et al., 2015). Its wide applicability comes from its competence in finding complex structures in high-dimensional data. Specifically, the capability of Deep Learning to learn a complex representation of images was enhanced by Convolutional Neural Network (CNN) which consists of two different layers: convolution and pooling layer. By convoluting adjacent values which are often highly correlated, CNN detects local motifs of the previous layer. Furthermore, its pooling layer reduces the dimension of the representation as well as creating robustness to small shift or noise. Through convolution layers and pooling layers, CNN can learn image representation hierarchically, combining lower level features to create higher-level features (Zeiler and Fergus, 2014). Recently, there have been further improvements on CNN architectures by utilizing a large image data (He et al., 2016; Huang et al., 2017; Krizhevsky et al., 2012; Simonyan and Zisserman, 2014; Szegedy et al., 2015).

Deep learning has proved its applicability in various medical image analysis tasks including medical image segmentation tasks (Litjens et al., 2017). Specifically, Ronneberger et al. have introduced U-Net by implementing VGG-Net like encoder as well as a mirrored decoder with convolution transpose layer (Ronneberger et al., 2015). Milletari et al. have extended U-Net for 3D data and introduced Dice Similarity Coefficient-based loss function for the segmentation of prostate volume in MRI (Milletari et al., 2016). However, automation of medical image analysis is challenging due to the inherent complexity of the medical image and extensive variation between patients (Hagerty et al., 2017). Such complexity and large variability within data call for a model with a large capacity which can discover more intricate structures of data. However, the complex model can suffer an overfitting unless it were trained with many samples with the i.i.d. assumption (Goodfellow et al., 2016). Unfortunately, in practice, image data are less available in the medical field than in other fields. As a result, overfitting can be a problem in building a network, especially for medical image analysis.

Various attempts have been proposed to moderate overfitting in Deep Learning such as batch normalization, drop-out, max-out, image augmentation, image normalization, etc (Goodfellow et al., 2013; Ioffe and Szegedy, 2015; Srivastava et al., 2014). In addition to these approaches, Multi-Task Learning (MTL) is known to improve model robustness and thus reduce the chance of overfitting (Goodfellow et al., 2016; Ruder, 2017). By adding an additional task, the parameters of the model are optimized towards values that can explain the variations observed in both tasks, reducing the chance of overfitting to the original task. Furthermore, the shared portion of the network can be constrained towards value with better generalization ability, if the additional task can provide information to the original task. As a result, MTL can reduce the risk of overfitting and allow the model to possess better generalization and robustness if the additional task is related to the original one.

Overfitting is often explained with the bias-variance decomposition of the expected loss (Goodfellow et al., 2016). Since overfitting is usually related to high variance (low model robustness), measuring model variance can be beneficial. Though mean squared error is usually used to explain the trade-off due

to its easy decomposition, the unified theorem of bias-variance decomposition also enabled arbitrary loss functions to be decomposed into noise, bias, and variance (Domingos, 2000).

In this paper, we proposed an MTL-based fully automatic method to segment both rectum and rectal cancer. In addition, we assumed that learning rectum would benefit learning rectal cancer, especially in overfitting considering their inherent geometrical correlation in addition to rectum's more consistent shape. Specifically, rectal cancer cannot appear far from rectum but mostly appear inside of rectum since rectal cancer grows from the rectum area (Cho et al., 2017). In our study, rectal cancer is always included in the rectum region since our dataset only covered rectal cancer with T3 or below (Gospodarowicz et al., 2017).

Our contributions in this work are as follows:

1. Utilizing Multi-Task Learning, we propose an encoder-decoder type segmentation network that simultaneously segments both rectum and rectal cancer. Automatic segmentation system for both rectum and rectal cancer can benefit current clinical procedure for treatment planning.
2. We prove that adding a rectum segmentation task can improve the performance of rectal cancer segmentation in our setting including a double residual connection.
3. We propose a bias-variance based method to visualize and assess the robustness of an image segmentation model
4. We present a novel augmentation method that can improve the segmentation performance especially trained with images with heterogeneous resolution.

2. Related Works

To the best of our knowledge, no study has been reported to suggest an auto-segmentation system of rectum using the MR image.

For rectal cancer segmentation system using MR images, Trebeschi et al. have proposed a patch-based training of convolutional neural network (CNN) model using both T2-weighted images and diffusion-weighted images (DWI) of MRI (Trebeschi et al., 2017). They sampled more patches from the regions with similar intensity value to that of rectal cancer and involved a post-processing step that only maintains the largest positive area (rectal cancer) to remove false positive pixels. The system can be inappropriate when more than one tumor exists in an image. Moreover, because 135 images were divided into training, validation, and test set without cross-validation, their evaluation could have suffered data selection bias.

In addition, we have not noticed any prior study reported that implements bias-variance decomposition in the field of image segmentation.

3. Method

3.1 Data Preparation

The experiments have been performed using MR images of patients with rectal cancer obtained between September 2004 and June 2016 at the National Cancer Center in South Korea. Out of 1813 patients, 457 patients were selected after disregarding the cases with at least one of the following

properties: cases with preoperative chemo-radiation, incomplete pathologic stage information, a contradiction between MR and pathologic stages, tumors located more than 13 cm or less than 3 cm from the anal verge or either clipping or stent states.

Rectal MR examinations were performed with one of four 3T or 1.5T superconducting systems (i.e., Achieva 3.0T (n = 233) and Achieva 3.0T TX (n = 131), Philips Healthcare, Cleveland, OH, USA; Signa HDX 3.0T (n = 19) and Genesis Signa 1.5T (n = 74), GE Healthcare, Milwaukee, WI, USA) using pelvic phased-array coils. Among the various MR imaging sequences, this experiment evaluated the axial T2-weighted fast-spin echo images.

Among approximately 30 image slices (per patient), one or two image slices were selected as our dataset. Selected images can clearly reflect the T-category of the patient containing rectum with the clear advent of either T2 or T3 rectal cancer. As a result, 907 MR images consist of 258 T2 images and 649 T3 images were selected. Two gastrointestinal clinical specialists were involved not only to select image slices but also to segment both rectum and rectal cancer for 907 images. These manual segmentation results are used as our ground truth. Specifically, one specialist drew the boundary, and the other specialist confirmed the segmentation outcome.

At last, 907 images were divided into 10 folds for 10-fold cross-validation as well as for bias-variance assessment. No fold shares the image from the same patient. For bias-variance assessment, we set apart the 10th fold as our test set and produced nine training set alike 9-fold cross-validation procedure. Note that we did not use the validation set alike 9-fold cross-validation but only used test set for bias-variance assessment which results in nine different prediction maps of the test set.

3.2 Preprocessing

Both image intensity range normalization and histogram equalization methods were applied in order to improve the image contrast as well as generalization (Drozdal et al., 2018). As a normalization step, both 90% maximum intensity value and the minimum intensity values from overall image slices of a patient were utilized to reduce the image depth from 12-bit to 8-bit. Contrast-limited adaptive histogram equalization (CLAHE) was also applied to enhance their contrast and reduce the effects of magnetic bias (Srivaramangai et al., 2017; Zuiderveld, 1994). As shown in Figure 1, the image with high-intensity artifact region which decreases the overall image contrast became more interpretable after preprocessing. In addition, all images were resized into 256×256 after the histogram equalization since the image-size of original MR images varies from 512×512 to 1056×1056 depending on the MR scanner.

During optimization, all training data went through random augmentation including adjusting the contrast, brightness, and sharpness followed by rotation, flipping (left and right), and cropping (maximum 10% from the edge and preserving the square shape). On the other hand, neither validation data nor test data (for bias-variance assessment) were augmented.

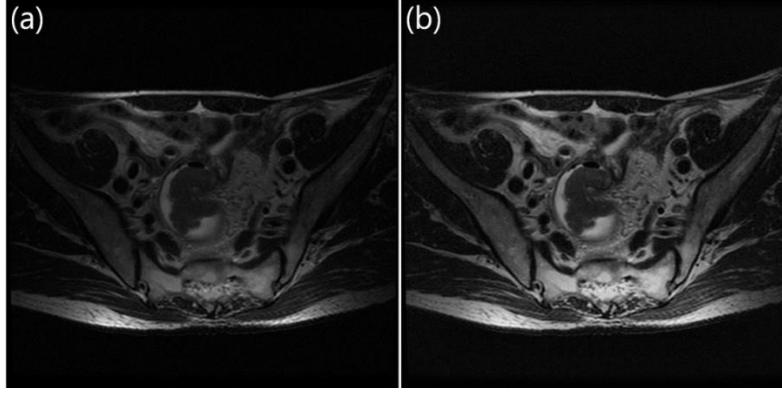


Figure 1 Example image before and after preprocessing: (a) original image and (b) pre-processed image.

3.3 Our Fully Convolutional Neural Network Approach

We implemented an encoder-decoder type segmentation network for the fully convolutional Multi-Task Learning (MTL). To segment both rectum and rectal cancer simultaneously, two task-specific 1×1 convolution layers are implemented in parallel as described in Figure 2.

The network involves seven convolution blocks between pooling layers and convolution transpose. For these seven blocks, we applied one of three different types of blocks specified in Figure 3 and compare their respective performances. In Figure 3, note that convolution block1 involves no residual skip connection whereas both convolution block2 and convolution block3 utilize residual skip connection in different ways. For both block2 and block3, we adopted pre-activation policy for every convolution layer as proposed by He et al (He et al., 2016). Moreover, the very first convolution layer of the network consists of $40 \ 3 \times 3$ filters. The number of filters at the encoder portion gets doubled after every convolution block alike VGG-Net or U-Net (Ronneberger et al., 2015; Simonyan and Zisserman, 2014). Decoder portion is a mirrored version of an encoder so that the number of filters is halved after each convolution block. More specifically, doubling or halving the number of filters is done by the first convolution in each block.

All filter weights were initialized using the normal distribution sampling method suggested by He et al. except the convolution transpose filter which was initialized using the uniform distribution sampling method suggested by Glorot and Bengio (Glorot and Bengio, 2010; He et al., 2015). Adam optimization algorithm was implemented to stochastically optimize the parameters with the mini-batch size of 20 (Kingma and Ba, 2014). Due to the imbalance number of negative pixels, we implemented Dice Similarity Coefficient (DSC)-based loss function suggested by Milletari et al. as our optimization objective function which is defined as follows (Milletari et al., 2016):

$$D = \frac{-2 \sum_i^N p_i g_i}{\sum_i^N p_i^2 + \sum_i^N g_i^2}$$

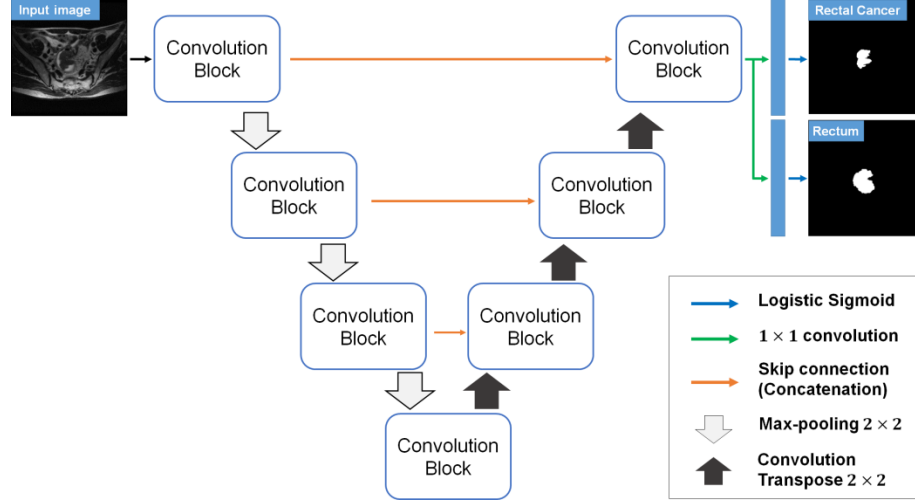


Figure 2 Fully Convolutional Network for Multi-Task Learning to segment both rectum and rectal cancer.

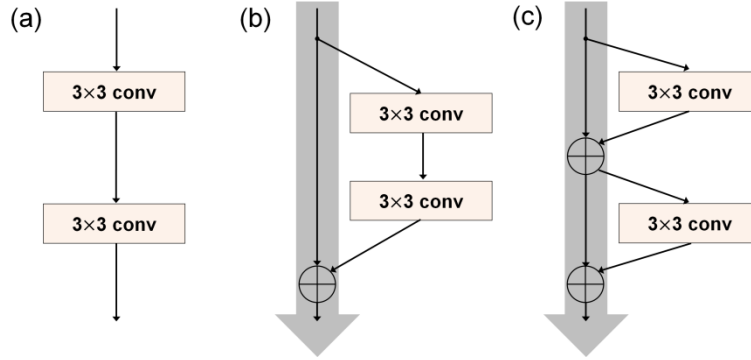


Figure 3 Three convolution blocks as our network backbone: (a) convolution block1, (b) convolution block2, and (c) convolution block3.

3.4 Performance Evaluation

Conventional 10-fold cross-validation was implemented in order to compare the performance of three network backbones for Multi-Task Learning (MTL) as well as between MTL and Single-Task Learning (STL). Furthermore, due to the excessive number of negative regions, we also utilized Dice Similarity Coefficient (DSC) as our metric to assess the similarity between the ground truth map and the prediction map in addition to the conventional sensitivity and specificity. DSC is defined as follows:

$$DSC(A, B) = \frac{2|A \cap B|}{|A| + |B|}$$

3.4.1. Bias-Variance Assessment

To assess how learning a rectum affects learning rectal cancer, we measured the bias, variance, and the expected loss per pixel generated by MTL and STL according to the unified definition (Domingos, 2000). However, the unified bias-variance decomposition suggested by Domingos involves an assumption that the true value t is a nondeterministic function of input x . As a result, the decomposition is done for the expected loss not only over the distribution of the training set D but also over the distribution of the true value t . According to the unified definition, the decomposition can be described as follows:

$$\begin{aligned} E_{D,t}[L(y^*, y)] &= c_1 E_t[L(t, y^*)] + L(y^*, y_m) + c_2 E_D[L(y_m, y)] \\ &= c_1 N(x) + B(x) + c_2 V(x) \end{aligned}$$

$N(x)$, $B(x)$, and $V(x)$ represent the noise of an example, the bias of a learner on example x , and the variance of a learner on example x , respectively. Moreover, y^* and y are the optimal prediction and the prediction of the learner, respectively. L is an arbitrary loss function (zero-one loss for our case) and $c_2 = 1$ if $y_m = y^*$ (unbiased), $c_2 = -1$ if biased. y_m is the main prediction which can be defined as follows:

$$y_m^{L,D} = \operatorname{argmin}_{y'} E_D[L(y, y')]$$

Because we decompose the expected loss of arbitrary pixel i , y_m will be the most frequent prediction for pixel i . Since we have nine different training sets, there will be no tie. Moreover, the proposed decomposition can be simplified as below considering 1) we have a deterministic ground truth for every training sample, and 2) we decomposed the loss at an arbitrary pixel i :

$$\begin{aligned} E_D[L(y^*(i), y(i))] &= L(y^*(i), y_m(i)) + c_2 E_D[L(y_m(i), y(i))] \\ &= B_i(x) + c_2 V_i(x) \end{aligned}$$

At last, because decomposition is done per pixel, we averaged the bias and variance over all pixel in an image as follows:

$$\begin{aligned} E_{D,i}[L(y^*(i), y(i))] &= E_i[L(y^*(i), y_m(i))] + c_2 E_{D,i}[L(y_m(i), y(i))] \\ &= E_i[B_i(x)] + E_i[c_2 V_i(x)] \end{aligned}$$

Since the variance negatively affects the expected loss of a biased pixel in opposition to the unbiased pixel, we also averaged the variance of biased pixels and unbiased pixels separately.

Overall, we measured the bias, variance, and expected loss per pixel in order to visualize the regional robustness via bias and variance. We also averaged these values to measure the expected value per pixel. Furthermore, these values were also averaged over positive (tumorous) region only due to the excessive number of pixels showing the area outside of a body which is unnecessary and predicted correctly at most of the time.

3.5 Image Size Augmentation

Because our dataset consists of images with various resolution, we aimed to enhance the robustness of our model in various resolution. As a result, we implemented a novel augmentation method which

randomly varies the image size of a mini-batch. Though we utilized the nature of the fully convolutional network which can accept various size of image as its input, we had to synchronize the size of all image within a mini-batch. Specifically, we randomly resized every mini-batch around 256x256 (from 192x192 to 288x288) considering that the image size of our validation set is fixed to 256x256. Images are kept square as all original images are square.

4. Result and Discussion

4.1 Network Backbone Selection

Table 1 presents the validation performance of the 10-fold cross-validation comparing the three different network backbones. As shown in the table, Block 3(convolution block3 in Figure 3) scored the highest Dice Similarity Coefficient (DSC) for both segmentation tasks (rectal cancer and rectum) with our proposed multi-task encoder-decoder network and thus was selected as our network backbone. Moreover, blocks with residual connection were trained faster than a block without residual connection. Among three blocks, Block 3 was trained faster than the other two blocks (Block 1: $\times 1.46$ more times, Block 2: $\times 1.04$ more times).

Table 1 Performance comparison of three different network backbones. All quantities are described as mean \pm standard deviation and were gathered through 10-fold cross-validation.

	DSC		Sensitivity		Specificity	
	Tumor	Rectum	Tumor	Rectum	Tumor	Rectum
Block 1	0.718 ± 0.201	0.935 ± 0.090	0.736 ± 0.225	0.932 ± 0.108	0.999 ± 0.002	0.999 ± 0.002
Block 2	0.722 ± 0.204	0.936 ± 0.092	0.741 ± 0.230	0.937 ± 0.105	0.999 ± 0.002	0.999 ± 0.002
Block 3	0.732 ± 0.195	0.938 ± 0.079	0.755 ± 0.221	0.936 ± 0.104	0.999 ± 0.002	0.999 ± 0.002

4.2 Comparing Multi-Task Network and Single-Task Network

With the network backbone selected, two Single-Task Learning (STL) networks for rectum segmentation and rectal cancer segmentation were trained. Figure 4 shows the example of learning progression of MTL as well as STL. Their respective performances were compared to the corresponding performances of Multi-Task Learning (MTL) network via 10-fold cross-validation as shown in Table 2. In addition to the segmentation performance, MTL network was trained faster than both STL networks. Specifically, the training of ten MTL networks (10-fold cross-validation) took $\times 0.96$ and $\times 0.81$ less time than training tumor STL network and rectum STL network on average, respectively.

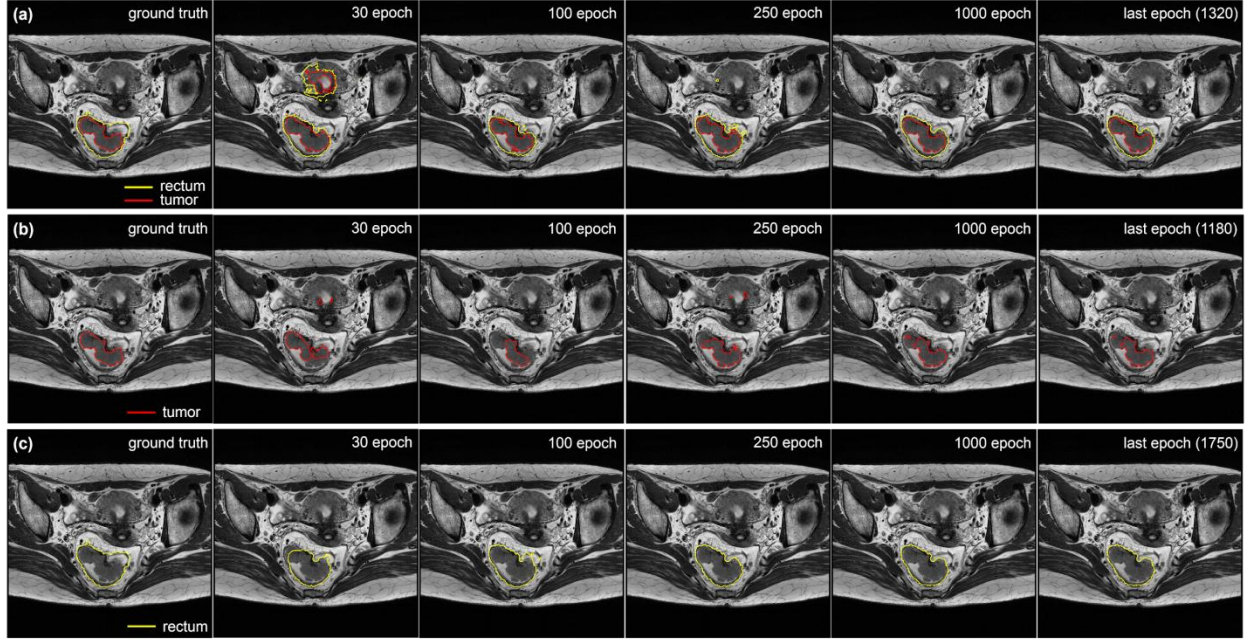


Figure 4 (a), (b), and (c) shows the learning progress of MTL, STL(tumor), STL(rectum), respectively. Note that the 6th column displays the prediction map of the last epoch.

Table 2 Performance comparison between STL and MTL. All quantities are described as mean \pm standard deviation and were gathered through 10-fold cross-validation.

	DSC		Sensitivity		Specificity	
	Tumor	Rectum	Tumor	Rectum	Tumor	Rectum
MTL	0.732 ± 0.195	0.938 ± 0.079	0.755 ± 0.221	0.936 ± 0.104	0.999 ± 0.002	0.999 ± 0.002
STL	0.723 ± 0.204	0.940 ± 0.088	0.743 ± 0.232	0.938 ± 0.107	0.999 ± 0.002	0.999 ± 0.002

Statistical analysis was done in order to validate the comparison in Table 2. Significant differences (paired t-test) between MTL and STL were observed in tumor DSC ($p=0.02$) as well as tumor sensitivity ($p=0.01$). All other distributions between MTL and STL were not significantly different.

4.3 Bias-Variance Assessment

In section 4.2, we confirmed with statistical test that our Multi-Task Learning (MTL) network outperformed our Single-Task Learning (STL) network in rectal cancer segmentation, and we aim to analyze their differences especially in robustness in this section.

In order to visualize how and in which region learning rectum improved learning rectal cancer especially in terms of robustness, we generated the bias and variance maps. Figure 5 shows the examples for nine different prediction maps which are used to get bias and variance maps.

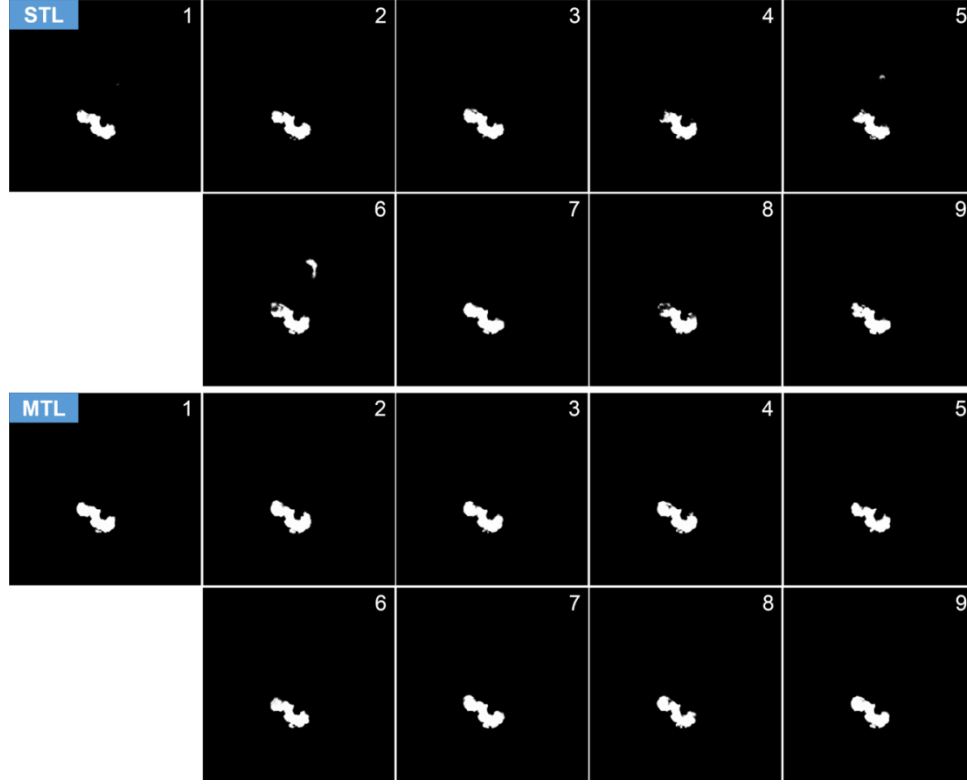


Figure 5 Nine rectal cancer prediction maps of the test sample. First two rows are the maps predicted by STL whereas the third and the fourth rows are from MTL. STL and MTL networks share training data only if the prediction number (located at the top right corner of each map) is the same. Each map is generated by the nine different training sets as described in section 3.2.

The variance of both STL and MTL network can be found in Figure 5. For example, at prediction maps 5 and 6, STL network made abnormal positive prediction far above the normal prediction region. Such regional model variance calls for a visualization method to assess the regional model robustness.

Figure 6 presents three examples of bias, variance, expected loss, and the ground truth maps overlaid with the input MR image. Because rectal cancer occupies only small portion in the image, we cropped predicted maps according to the yellow box in column (d) only for the visualization purpose. Note that yellow arrows show the notable difference between STL and MTL.

Most bias and variance occurred at the boundary of rectal cancer. However, STL occasionally showed less robustness at other organs with similar in shape and intensity at MR image. Moreover, within the rectal cancer region, STL showed more variance which is notable with the bottommost example.

Furthermore, we measured the bias ($E[\text{Bias}]$), variance ($E[\text{Var}_{\text{Total}}]$), and expected loss ($E[L]$) of STL and MTL at a pixel and compared their distributions. Table 3 showed that learning rectum decreased both bias and variance in rectal cancer segmentation with statistically significant decrease in variance ($p=0.0002$). Note that learning rectum increased the variance in biased pixel ($E[\text{Var}_{\text{Biased}}]$) whereas it significantly reduced the variance of unbiased pixel ($E[\text{Var}_{\text{Unbiased}}]$) ($p=2.78e-5$). Learning rectum altered bias, the variance of biased pixels, and the variance of unbiased pixels in a way to reduce the expected loss. The expected loss was significantly reduced from STL to MTL ($p=0.0002$). Note that the variance of biased pixels affects the expected loss negatively.

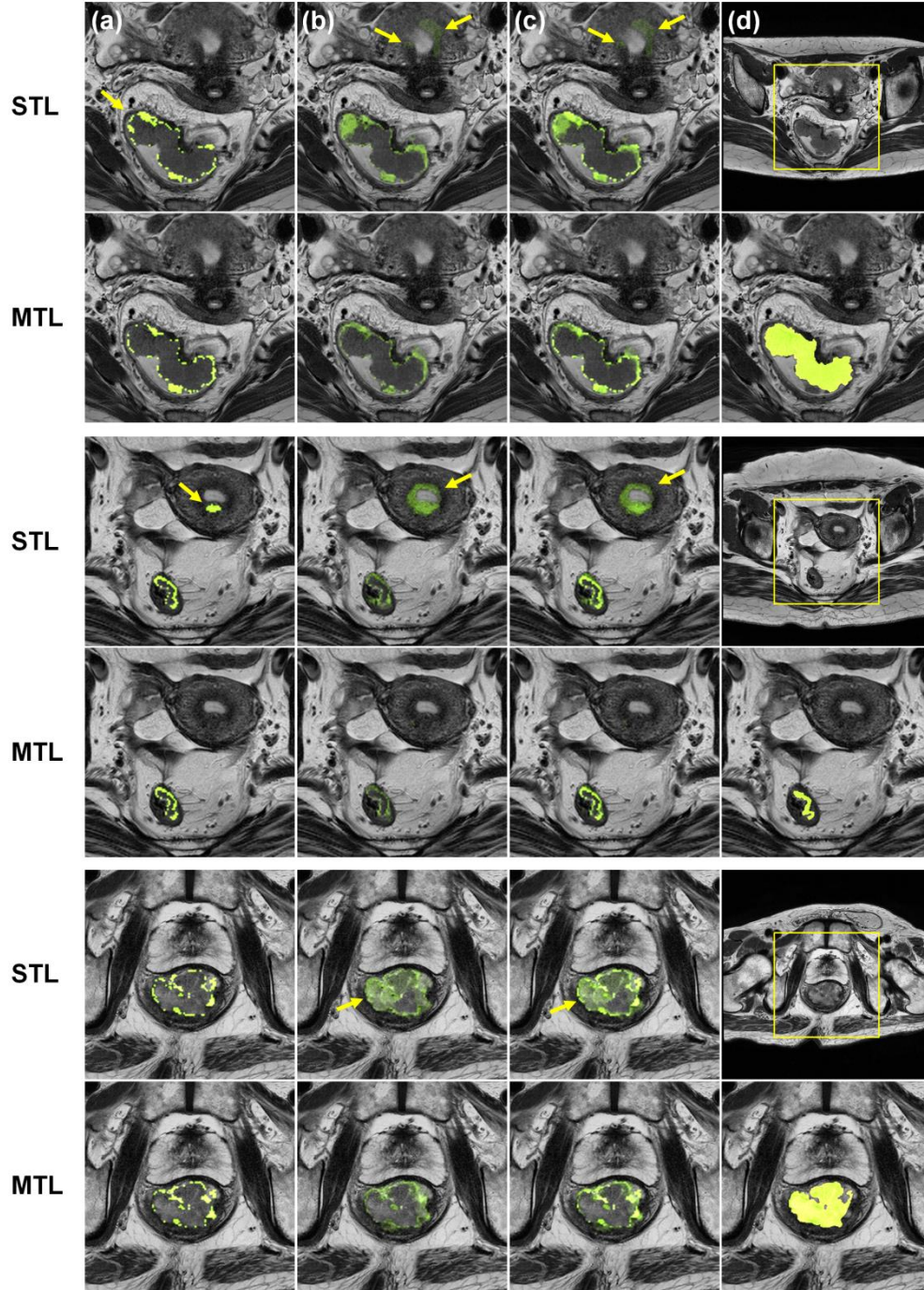


Figure 6 Three test examples with their bias (a), variance (b), and expected loss (c) maps by STL and MTL. Column (d) shows the original image with the yellow box to crop as well as the ground truth. Note that the uppermost example corresponds with Figure 5, and the regional variance of STL at other organ is captured by the variance map as well as the expected loss map.

Table 3 Expected bias, expected variance (total, biased, unbiased), and expected zero-one loss for positive region and overall region.

		E[Bias]	E[Var _{Total}]	E[Var _{Biased}]	E[Var _{Unbiased}]	E[L]
Positive	STL	0.248 ±0.232	0.093 ±0.065	0.189 ±0.089	0.091 ±0.080	0.272 ±0.225
	MTL	0.232 ±0.232	0.084 ±0.054	0.200 ±0.183	0.075 ±0.058	0.246 ±0.214
Total	STL	0.003 ±0.004	0.001 ±0.001	0.180 ±0.071	0.001 ±0.001	0.003 ±0.004
	MTL	0.003 ±0.004	0.001 ±0.001	0.183 ±0.069	0.001 ±0.001	0.003 ±0.004

Table 4 Performance comparison of MTL with and without the image size augmentation method. All quantities are described as mean ± standard deviation and were gathered through 10-fold cross-validation.

	DSC		Sensitivity		Specificity	
	Tumor	Rectum	Tumor	Rectum	Tumor	Rectum
MTL	0.732 ±0.195	0.938 ±0.079	0.755 ±0.221	0.936 ±0.104	0.999 ±0.002	0.999 ±0.002
MTL-AUG	0.746 ±0.186	0.944 ±0.070	0.770 ±0.214	0.941 ±0.095	0.999 ±0.002	0.999 ±0.002

4.4 Image Size Augmentation

We measured the efficacy of our image size augmentation on our Multi-Task Learning (MTL) network through 10-fold cross-validation. The augmentation improved the performance of both rectum and rectal cancer segmentation with significant difference in DSC in tumor ($p=8.84e-5$), DSC in rectum ($p=1.02e-5$), sensitivity in tumor ($p=0.0003$), sensitivity in rectum ($p=0.001$), and specificity in rectum ($p=0.016$). In addition, the augmentation reduced the average training duration approximately x0.78 times.

5. Result and Discussion

In this study, we presented a fully automatic method to segment both rectum and rectal cancer simultaneously using T2-weighted axial MR image. Automatic segmentation system for both rectum and rectal cancer is expected to expedite the current manual localization procedure by radiologists as well as to assist professionals to classify the T-categories of rectal cancer for treatment planning.

We also proposed a method to visualize regional model robustness of image segmentation network. Moreover, we measured the expected bias, expected variance, and the expected loss of an image by

following the unified definition. Our proposed assessment can be especially beneficial to evaluate a complex model trained with a limited number of images, which often suffers from overfitting. At last, we also presented an augmentation method which is aimed to improve model robustness at different resolutions by randomly resizing the image size of mini-batch.

Through 10-fold cross-validation, our proposed network trained with image size augmentation method scored Dice Similarity Coefficient (DSC) of 0.746 and 0.944 in rectal cancer segmentation and rectum segmentation, respectively. The score surpassed the current state-of-the-art for tumor segmentation which scored around 0.69 in DSC (Trebeschi et al., 2017) whereas there has been no previous report for rectum segmentation using axial MR image. Our method is also computationally efficient due to its fully convolutional architecture (i.e., 0.006 seconds per image to segment both rectum and rectal cancer).

Acknowledgments

This project was supported by the grant from the National Cancer Center (NCC-1710070).

References

- Arnold, M., Sierra, M.S., Laversanne, M., Soerjomataram, I., Jemal, A., Bray, F., 2017. Global patterns and trends in colorectal cancer incidence and mortality. *Gut* 66, 683-691.
- Bhandari, A., Woodhouse, M., Gupta, S., 2017. Colorectal cancer is a leading cause of cancer incidence and mortality among adults younger than 50 years in the USA: a SEER-based analysis with comparison to other young-onset cancers. *Journal of Investigative Medicine* 65, 311-315.
- Cho, S.H., Cho, Y.S., Choi, I.Y., Ha, H.I., Huh, J., Hur, B.Y., Hwang, J., Jang, H.Y., Kim, A.Y., Kim, A.Y., 2017. Essential. Items for Structured Reporting of Rectal. Cancer MRI: 2016 Consensus Recommendation from the Korean Society of Abdominal. Radiology. *KOREAN JOURNAL OF RADIOLOGY* 18, 132-151.
- Domingos, P., 2000. A unified bias-variance decomposition, *Proceedings of 17th International Conference on Machine Learning*, pp. 231-238.
- Drozdal, M., Chartrand, G., Vorontsov, E., Shakeri, M., Di Jorio, L., Tang, A., Romero, A., Bengio, Y., Pal, C., Kadoury, S., 2018. Learning normalized inputs for iterative estimation in medical image segmentation. *Medical image analysis* 44, 1-13.
- Glorot, X., Bengio, Y., 2010. Understanding the difficulty of training deep feedforward neural networks, *Proceedings of the thirteenth international conference on artificial intelligence and statistics*, pp. 249-256.
- Goodfellow, I., Bengio, Y., Courville, A., Bengio, Y., 2016. *Deep learning*. MIT press Cambridge.
- Goodfellow, I.J., Warde-Farley, D., Mirza, M., Courville, A., Bengio, Y., 2013. Maxout networks. *arXiv preprint arXiv:1302.4389*.
- Gospodarowicz, M.K., Brierley, J.D., Wittekind, C., 2017. *TNM classification of malignant tumours*. John Wiley & Sons.
- Hagerty, J., Stanley, R.J., Stoecker, W.V., 2017. *Medical Image Processing in the Age of Deep Learning*.

- He, K., Zhang, X., Ren, S., Sun, J., 2015. Delving deep into rectifiers: Surpassing human-level performance on imagenet classification, Proceedings of the IEEE international conference on computer vision, pp. 1026-1034.
- He, K., Zhang, X., Ren, S., Sun, J., 2016. Identity mappings in deep residual networks, European conference on computer vision. Springer, pp. 630-645.
- Huang, G., Liu, Z., Van Der Maaten, L., Weinberger, K.Q., 2017. Densely connected convolutional networks, 2017 IEEE Conference on Computer Vision and Pattern Recognition (CVPR). IEEE, pp. 2261-2269.
- Ioffe, S., Szegedy, C., 2015. Batch normalization: Accelerating deep network training by reducing internal covariate shift. arXiv preprint arXiv:1502.03167.
- Jung, K.-W., Won, Y.-J., Oh, C.-M., Kong, H.-J., Lee, D.H., Lee, K.H., 2017. Prediction of cancer incidence and mortality in Korea, 2017. Cancer research and treatment: official journal of Korean Cancer Association 49, 306.
- Kingma, D.P., Ba, J., 2014. Adam: A method for stochastic optimization. arXiv preprint arXiv:1412.6980.
- Krizhevsky, A., Sutskever, I., Hinton, G.E., 2012. Imagenet classification with deep convolutional neural networks, Advances in neural information processing systems, pp. 1097-1105.
- LeCun, Y., Bengio, Y., Hinton, G., 2015. Deep learning. nature 521, 436.
- Litjens, G., Kooi, T., Bejnordi, B.E., Setio, A.A.A., Ciompi, F., Ghafoorian, M., Van Der Laak, J.A., Van Ginneken, B., Sánchez, C.I., 2017. A survey on deep learning in medical image analysis. Medical image analysis 42, 60-88.
- Milletari, F., Navab, N., Ahmadi, S.-A., 2016. V-net: Fully convolutional neural networks for volumetric medical image segmentation, 3D Vision (3DV), 2016 Fourth International Conference on. IEEE, pp. 565-571.
- Ronneberger, O., Fischer, P., Brox, T., 2015. U-net: Convolutional networks for biomedical image segmentation, International Conference on Medical image computing and computer-assisted intervention. Springer, pp. 234-241.
- Ruder, S., 2017. An overview of multi-task learning in deep neural networks. arXiv preprint arXiv:1706.05098.
- Simonyan, K., Zisserman, A., 2014. Very deep convolutional networks for large-scale image recognition. arXiv preprint arXiv:1409.1556.
- Srivaramangai, R., Hiremath, P., Patil, A.S., 2017. Preprocessing MRI Images of Colorectal Cancer. International Journal of Computer Science Issues (IJCSI) 14, 48.
- Srivastava, N., Hinton, G., Krizhevsky, A., Sutskever, I., Salakhutdinov, R., 2014. Dropout: a simple way to prevent neural networks from overfitting. The Journal of Machine Learning Research 15, 1929-1958.
- Szegedy, C., Liu, W., Jia, Y., Sermanet, P., Reed, S., Anguelov, D., Erhan, D., Vanhoucke, V., Rabinovich, A., 2015. Going deeper with convolutions, Proceedings of the IEEE conference on computer vision and pattern recognition, pp. 1-9.
- Trebeschi, S., van Griethuysen, J.J., Lambregts, D.M., Lahaye, M.J., Parmer, C., Bakers, F.C., Peters, N.H., Beets-Tan, R.G., Aerts, H.J., 2017. Deep learning for fully-automated localization and segmentation of rectal cancer on multiparametric MR. Scientific reports 7, 5301.
- Zeiler, M.D., Fergus, R., 2014. Visualizing and understanding convolutional networks, European conference on computer vision. Springer, pp. 818-833.
- Zuiderveld, K., 1994. Contrast limited adaptive histogram equalization. Graphics gems, 474-485.